On clarification of haze in polypropylene

On Clarification of Haze in Polypropylene

Karin Bernland,[1] J. G. P. Goossens,[2] Paul Smith,[1] Theo A. Tervoort[1]

[1]Department of Materials, ETH Zurich, Zurich 8093, Switzerland
[2]Department of Chemical Engineering and Chemistry, Eindhoven University of Technology, PO Box 513, MB Eindhoven 5600, The Netherlands
Correspondence to: T. A. Tervoort (E-mail: theo.tervoort@mat.ethz.ch)

Received 2 November 2015; accepted 14 December 2015; published online 19 January 2016
DOI: 10.1002/polb.23992

ABSTRACT: The mechanism of reducing light scattering in isotactic polypropylene (*i*-PP), through the addition of so-called clarifying agents, is studied with small-angle light scattering (SALS) and scanning electron microscopy (SEM). The clarifying agents used in this study depict monotectic phase behavior with *i*-PP, crystallizing in a relatively narrow concentration range in a nanofibrillar network, providing an ultrahigh nucleation density in the *i*-PP melt. It is found that the clarifying effect, a dramatically increased transparency and reduced haze, that occurs within the aforementioned additive concentration range, coincides with a change in morphology from strongly scattering spherulites to shish-kebab-like crystalline structures, as evidenced by *in situ* SALS measurements and confirmed by SEM images. A simple scaling law, relating the diameter of the shish-kebab structures to the fibril diameter and volume fraction of the clarifying agent is proposed, suggesting that the performance of a (fibril-forming) clarifying agent will improve by reducing the fibril diameter and/or increasing the volume concentration of the clarifying agent. © 2016 Wiley Periodicals, Inc. J. Polym. Sci., Part B: Polym. Phys. **2016**, *54*, 865–874

KEYWORDS: clarifying agents; isotactic polypropylene; light scattering; poly(propylene); nucleation; SALS; spherulites; transparency

INTRODUCTION Additives are increasingly used to introduce various favorable properties upon commodity polymers, turning them into valuable high-performance materials.[1] For example, small amounts of so-called clarifying agents transform normally opaque or translucent isotactic polypropylene (*i*-PP) into a transparent material, therewith opening up a range of new applications, especially in the packaging industry. Due to their great utility, significant research efforts have been, and still are, devoted to developing new, more efficient and more versatile clarifying agents.[2–6]

Clarifying agents typically consist of small molecules that exhibit monotectic phase behavior with the polymer matrix,[7–9] dissolving at elevated temperatures in the polymer melt and crystallizing into nanofibrils or a nanofibrillar network upon quenching, thus providing a very large surface area for the polymer matrix to nucleate upon. In this way, it has been argued that clarifying agents drastically increase the nucleation density, thereby reducing the size of the spherulites that are responsible for the scattering of light, resulting in a more transparent material. This traditional view was confirmed in recent studies, where it was found that optical transparency indeed correlates with nucleation density rather than nucleating efficiency.[10,11] However, the precise morphological requirements for clarification are still a matter of debate, and relatively few studies have been directed to resolve the detailed microscopic structure of clarified semi-crystalline polymers. Vaughan and Hosier[12] used scanning electron microscopy (SEM) and differential scanning calorimetry (DSC) to evaluate the effect of a commercial clarifying agent, (1,3:2,4) dibenzylidene sorbitol (DBS), on the morphology and crystallization kinetics of blends of linear and branched polyethylene. It was found that DBS greatly enhances nucleation in polyethylene and that, following phase separation at high crystallization temperatures, the rejected low molar mass polyethylene decorated the DBS network to form shish-kebab-like structures. Nogales and Mitchell also observed shish-kebab structures upon shearing a propylene/ethylene copolymer containing DBS.[13–15] Lipp et al.[16] used transmission electron microscopy (TEM) and small-angle X-ray scattering (SAXS) to determine the kinetics of nanofibril formation of 1,3:2,4-di(3,4-dimethylbenzylidene) sorbitol (DMDBS) in an *i*-PP matrix. Schmidt et al.[17] used ^{13}C DQ solid-state NMR spectroscopy to probe the columnar structure of self-assembled 1,3,5-benzenetrisamides, a new clarifying agent, in isotactic polypropylene. Andreassen et al.[18] analyzed the effect of clarifying agents on the haze of polyethylene using atomic force microscopy (AFM) and identified row-nucleated structures in samples with reduced haze.

An important experimental tool to study the interaction of light with matter is small-angle light scattering (SALS), which has often been used to explore and model polymer morphology, especially in early stages of crystallization.[19–26] As optical transparency and perceived clarity of semi-crystalline polymers are determined by the angular dependence of the scattered light, SALS seems also an ideal technique to study clarification of polymers. This notwithstanding, SALS has only been used sparsely in connection with clarifying agents.[27–30] Johnsen and Spilgies[27] used small-angle light scattering (SALS) to examine the morphology of *i*-PP nucleated with aluminum hydroxy *bis*(4-*tert*-butyl) benzoate, and observed a transition from a spherulitic to a supramolecular structure consisting of cross-hatched quadrites. Garg et al. employed SALS to study the clarification of *i*-PP with DBS to find that the orientation of the crystals relative to the spherulite radius decreased and that the nucleating agent agglomerated with increasing concentration in the polymer.[28,29] Kobayashi and Hashimoto[30] conducted SALS on *i*-PP clarified with 1,3:2,4-*bis*-*O*-(*p*-methylbenzylidene)-D-sorbitol (PDTS) and observed scattering patterns that were indicative of rod-like scattering rather than spherulitic scattering. All these studies seem to indicate that a nanofibrillar structure and the associated high nucleation density are the key ingredients that make up an efficient clarifying agent, although more precise guidelines are still missing. It is the objective of this study to use SALS together with scanning electron microscopy (SEM) and optical microscopy for an in-depth investigation of the morphology of *i*-PP as a function of clarifier concentration, for a series of commercial and new clarifying and nucleating agents, to identify in more detail microstructural aspects that are important for the improvement of haze and clarity during clarification of *i*-PP.

EXPERIMENTAL

Materials

The isotactic polypropylene used was Moplen HF 500N from Basell ($M_n = 76$ kg/mol, $M_w = 260$ kg/mol, PDI = 3.5). The clarifying agent (**1**) 1,3:2,4-*bis*(3,4-dimethyl-benzylidene)sorbitol (DMDBS, Millad 3988, CAS Registry Number: 135861-56-2) was used as received from Milliken Chemicals, and (**2**) 1,2,3-trideoxy-4,6:5,7-*bis*-*O*-[(4-propylphenyl)methylene]-nonitol (TBPMN, NX8000, CAS Registry Number: 882073-43-0) was synthesized according to general procedures in Xie et al.[31] The clarifying agent (**3**) 1,3,5-*tris*(2,2-dimethylpropionylamino)benzene (Irgaclear XT386, CAS Registry Number: 745070-61-5) was used as received from Ciba Specialty Chemicals. The additive (**4**) *N*,*N*′-*bis*(1-methylethyl)−5-(2-methylpropionylamino)isophtalamide (CAS Registry Number: 1217310-08-1) was kindly provided by the group of Prof. Dr. Hans-Werner Schmidt, University of Bayreuth, Germany, where it was synthesized according to Abraham et al.[5] The chemical structures of the additives **1**-**4** are listed in Table 1, together with selected characteristic properties.

TABLE 1 Chemical Structures of Additives used in this Study: 1, 1,3:2,4-*Bis*(3,4-dimethyl benzylidene)sorbitol; 2, 1,2,3-Trideoxy-4,6:5,7-*bis*-*O*-[(4-propylphenyl) methylene]-nonitol; 3,1,3,5-*Tris*(2,2-dimethylpropionylamino)benzene; 4, *N*,*N*′-*Bis* (1-methylethyl)−5-(2-methyl-propionylamino)isophtalamide

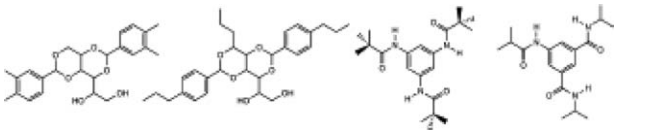

Add.	–	1	2	3	4
% w/w	0	1	1	0.025	0.07
H (%)	71	15	9	16	58
C (%)	49	98	96	98	81
T_c (°C)	113	131	131	125	119

The table lists the values of haze (*H*), clarity (*C*), and peak crystallization temperature, T_c, of neat *i*-PP (left), and comprising the different additives at contents where minimum haze was observed. The *i*-PP β-crystal modification content is $\leq$ 10% in all samples

Thermal Analysis

Thermal analysis was conducted using a differential scanning calorimeter (DSC 822e, Mettler Toledo, Switzerland) calibrated with Indium for temperature and enthalpy. DSC thermograms were recorded under nitrogen at standard heating and cooling rates of 10 °C/min; the sample weight was about 10 mg. The degree of crystallinity of the polymer was calculated from the enthalpy of fusion, derived from the endothermic peak, adopting a value of 207.1 J/g for 100% crystalline isotactic polypropylene.[32]

Haze and Clarity Measurements

The characteristics often used to quantify the optical properties of a material with respect to its transparency are haze and clarity. Haze is defined as that part of the total amount of transmitted light which is scattered at angles higher than 2.5°, normalized by the incoming flux.[33] A high value of haze signifies a loss of contrast of an object viewed through the material. Clarity, which refers to the ability of a material to transmit fine details of an artifact, is more difficult to assess and there are several different methods of quantification.[33] In this study, therefore, macroscopic optical properties will mainly be characterized by the value of haze. Haze measurements were performed on 1 mm thick injection-molded circular samples, using a BYK-Gardner haze guard plus with CIE illuminant C according to ASTM D-1003. Clarity was measured on the same machine as the total amount of transmitted light which is scattered at angles smaller than 2.5°, normalized by the incoming flux.

Sample Preparation

Blends of *i*-PP comprising varying amounts of the additives were compounded in a laboratory co-rotating mini-twin-screw extruder (Eindhoven University of Technology, the Netherlands) at 100 rpm for 10 min under a nitrogen

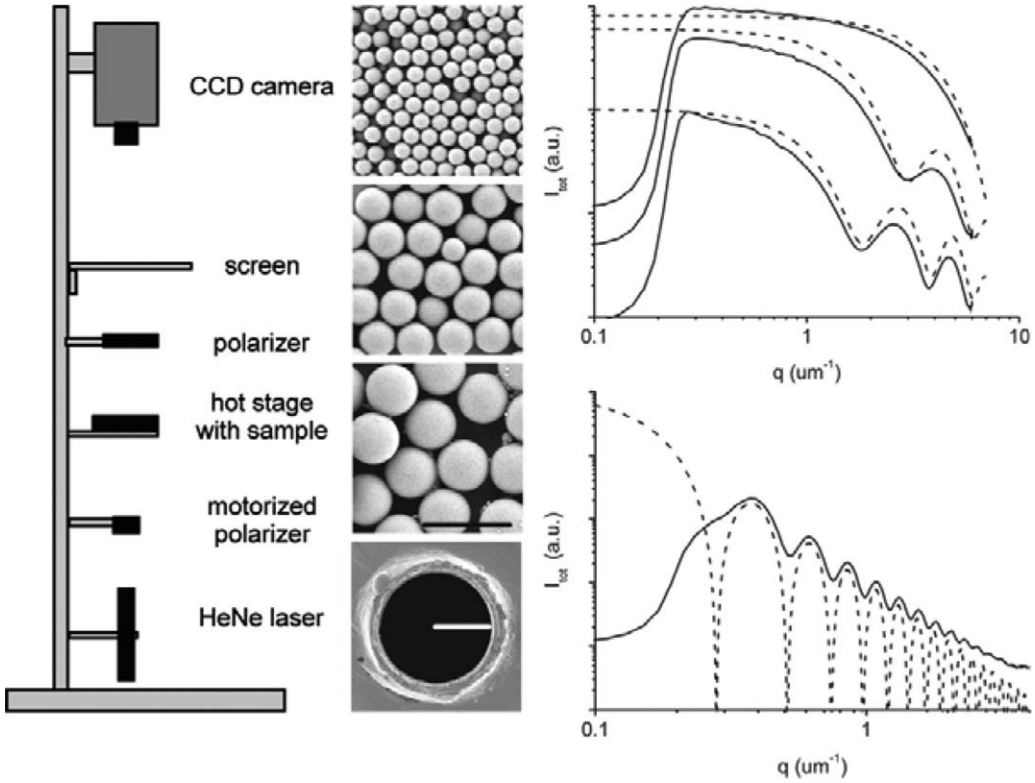

FIGURE 1 Left: Schematic of the equipment employed for small-angle light scattering (SALS) studies. Center: Scanning electron microscopy (SEM) images of dried suspensions of polystyrene (PS) particles (scale bar 5 μm) and pinhole (radius = 13.7 μm) used for calibration. Top right: Log-log plot of the integrated scattering (I_{tot}) from the PS spheres in suspension (-) together with that calculated according to the Mie model for scattering from spheres[38] with, from top to bottom, average diameter, d_{av} = 1.04, 2.05, and 3.10 μm (- - -). The curves have been shifted along the *y*-axis for clarity. Bottom right: Log-log plot of the integrated intensity (I_{tot}) by the pinhole (-) and calculated with the Airy function[37] for a pin diameter = 27.4 μm (- - -).

blanket at 230 °C. Reference samples of the neat polymer were produced in the same way. The samples for small-angle light scattering (SALS) investigations were prepared by melt-compression molding previously compounded material between two glass slides, followed by quenching to room temperature. The molding temperature was adapted to the additive characteristics and concentration to ensure complete melting of the agent, and ranged from 230 °C to 290 °C. Poly(tetrafluoroethylene) (PTFE) spacers were used to produce a homogeneous sample thickness of 0.1 mm.

The samples for the haze and clarity measurements were prepared by injection molding, using a laboratory mini-injector (DACA instruments, Santa Barbara, CA). The material was molten and kept 2 min at 240 °C under a nitrogen blanket before injection in the mold, which was held at room temperature. Polished molds were used to minimize the influence of scattering due to surface roughness on the haze values.

Small-Angle Light Scattering

The experimental set up used for small-angle light scattering studies is shown in Figure 1. A He-Ne laser (λ=632.8 nm, JDL 1125P, JDS Uniphase) is directed through the sample and the resulting scattering pattern is projected onto a screen (Marata plate, Linos, Germany). The scattering pattern is recorded with a CCD camera (PIXIS 512, Princeton Instruments), connected to a data acquisition system.[34,35] The lower polarizer is mounted on a motorized stage, enabling crossed and parallel positions of the polarizers (H_V and V_V orientation, respectively). The scattered intensities were recorded as a function of scattering angle θ and azimuthal angle μ (see Fig. 2). Calibration of the scattering angle was performed using a grating. The images were corrected for

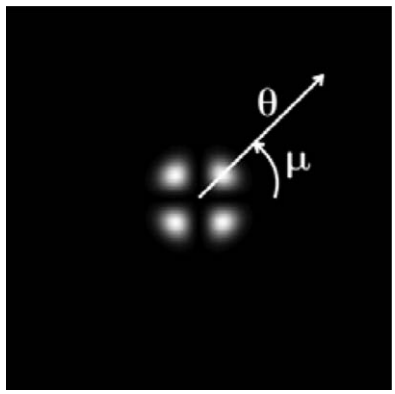

FIGURE 2 Schematic H_V-scattering pattern of a spherulite, showing the radial angle θ and azimuthal angle μ.

flat-screen projection and background noise before analyzing the data. A dark-current image recorded directly after the measurement with equal acquisition time was used as dark image and subtracted pixel by pixel, thereby also correcting for detector sensitivity. All images were recorded at constant beam intensity and sample-to-screen distance, and were corrected for reflection and refraction according to the method described by Stein and Keane.[36]

The set-up was calibrated using a pinhole as well as (quasi-) monodisperse latex suspensions of polystyrene (PS) microspheres of diameters of approximately 1, 2, and 3 μm, respectively (see Fig. 1). The exact diameters of the pinhole and the particles in suspension were determined by scanning electron microscopy (SEM) before the SALS measurements. A comparison of the integrated experimental scattering pattern obtained from the pinhole with the theoretical diffraction pattern given by the Airy function[37] shows good correlation for scattering vectors up to 3 μm^{-1}. Similarly, the experimental scattering patterns for the suspensions are found to correspond well with the Mie model[38] of scattering from perfect spheres within the measured range. Typically, at least two measurements were conducted in each experiment to warrant reproducibility. Finally, it should be noted that the SALS images in Figures 4, 6–8 are inverted and rescaled for best possible contrast, hence, the intensity levels in these images cannot be compared directly.

The two-dimensional scattering pattern can be used to identify different aspects of the specific microstructure. For example, H_V-scattering patterns of perfect spherulites with radius $\bar{r}_s$ display a characteristic four-clove pattern (see Fig. 2), with maxima at θ_{max} at azimuthal angles of 45°, that allow an estimation of the average spherulite radius $\bar{r}_s$ using the following equation:[39,40]

$$\bar{r}_s = \frac{4.09\lambda}{4\pi \sin(\theta_{max}/2)} \quad (1)$$

After circular integration over the azimuthal angle μ and averaging over the number of pixels, the scattered H_V and V_V intensities, I_{H_V} and I_{V_V}, were evaluated as a function of the scattering vector, q, defined as:

$$q = \frac{4\pi}{\lambda} \sin\left(\frac{\theta}{2}\right) \quad (2)$$

Here λ and θ are, respectively, the wavelength of light and the scattering angle in the medium containing the scattering entities (i.e. *i*-PP). The circular integration was performed using the Fit2D program.[41] Assuming perfect polarizers, the total scattered intensity was calculated as the sum of the H_V- and V_V-scattered intensities: $I_{tot}(q) = I_{H_V}(q) + I_{V_V}(q)$. By limiting the integration of the total scattered intensity to scattering angles θ higher than 2.5°, we obtain a value, $I_{2.5}$, which will serve as an approximate measure of haze (see above), even though it is not normalized. Circularly integrated intensities were integrated over the experimentally accessible q-range, to obtain the so-called invariant Q, defined as $Q = \int_0^\infty I(q) q^2 dq$. In case of spherulitic crystallization, neglecting both the amorphous contribution to the spherulite polarization anisotropy and the form anisotropy, it has been shown that, at small angles, the invariant for H_V configuration, Q_δ, effectively probes the mean-square fluctuations in anisotropy $\langle \delta^2 \rangle$, and is given by:[40,42,43,51]

$$Q_\delta = \frac{K}{15} \langle \delta^2 \rangle = \frac{K}{15} \phi_{sp} \left(\phi_{csp} \delta^0_{cr} P_2\right)^2 \quad (3)$$

Here, K is a constant, ϕ_{sp} is the volume fraction of spherulites, ϕ_{csp} is the volume fraction crystallinity within a spherulite, δ^0_{cr} is the intrinsic anisotropy of a pure crystal and P_2 is a Hermans-type orientation function describing the orientation of the crystalline segments with respect to the spherulite radius,[43,51] having a limiting value of 1 for perfectly arranged spherulites. From eq 3, it follows that, even though the invariant is independent of the size of the spherulites, it does depend on their internal molecular orientation (or organization), where disordering will result in a system of less scattering power,[42] as is the case for co-polymers.[44] Furthermore, this research is only concerned with the case of space-filling spherulitic crystallization, $\phi_{sp} = 1$, so that Q_δ reduces to:[43,51]

$$Q_\delta = \frac{K}{15} \left(\phi_{csp} \delta^0_{cr} P_2\right)^2, \quad (4)$$

from which it follows that, in case of space-filling spherulitic crystallization, irrespective of the spherulite size, Q_δ is constant as long as the crystallinity and orientation of the crystallites within the spherulites are constant.

Scanning Electron Microscopy

Samples for scanning electron microscopy (SEM) studies were prepared by casting a solution of ≈ 1% w/(w solvent) of *i*-PP, containing 1% w/(w polymer) solid additive (2% w/(w polymer) solid for compound **4**), in *p*-xylene, yielding thin films after evaporation of the solvent, typically of about 10 μm thickness. These films were subsequently molten and quenched to room temperature in the same manner as the compression-molded samples for SALS analysis. The samples thus produced were coated with a thin conductive microscope layer of platinum and imaged using a LEO 1530 Gemini (LEO Elektronenmikroskopie GmbH, Germany).

RESULTS AND DISCUSSIONS

Pristine *i*-PP

Two-dimensional scattering diagrams for pristine *i*-PP are shown in Figure 3, one for a sample crystallized at a moderate cooling rate, resulting in relatively large spherulites due to the reduced rate of nucleation at low undercooling, and one for a sample quenched in ice water, resulting in substantially smaller spherulites, due to the increased rate of nucleation at larger undercooling. As can be seen in Figure 3, both scattering patterns depict the typical scattering pattern for spherulites as shown in Figure 2. Using eq 1, the average spherulite radii $\bar{r}_s$ are estimated at about 13 μm for the

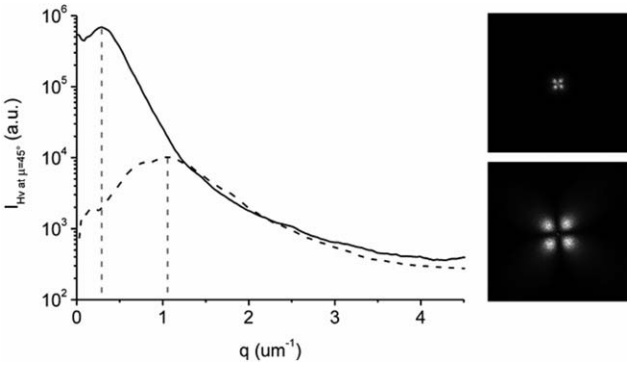

FIGURE 3 Right: Scattering patterns under crossed polarizers (H_V) for *i*-PP quenched to room temperature (top) and in ice water (below). Left: Scattered intensity at azimuthal angle 45° versus scattering vector q of the ice-water (dashed line) and room-temperature quenched (solid line) sample, where the indicated maxima correspond to $\bar{r}_s$=13 μm and $\bar{r}_s$=4 μm, respectively.

slower cooled and 4 μm for the quenched sample, respectively.

Light Scattering as a Function of Additive Concentration

It is well known from earlier studies that the ability of an additive to clarify is closely linked to the phase behavior of the polymer/additive system.[2,7] Hence, performing SALS investigations of a series of *i*-PP samples containing a relevant range of concentrations of the commercial clarifying agent **1**, allows for a direct determination of the effect of the clarifying agent on the polymer's morphology at different stages and how this correlates with various optical properties. Only space-filling systems are considered and, therefore, the focus is on the scattering of light detected under crossed polarizers. According to DSC measurements the crystallinity of *i*-PP is not influenced much by the addition of **1**; thus, changes in Q_δ are only due to variations in the internal orientation or shape of the crystallites and, consequently, provide a direct indication of changes in their structure and arrangement.

In Figure 4, SALS images, obtained using crossed polarizers, of *i*-PP containing different amounts of **1** are displayed, together with plots of $I_{2.5}$ and Q_δ versus the composition of the corresponding samples. Similar as for the macroscopic optical properties, "haze" and "clarity," three concentration regimes can be discerned.[7] Initially, at low concentrations of the additive (0–0.15% w/w), scattering typical of spherulitic structures is dominating. That pattern becomes successively larger, indicating that the spherulite size is decreasing. The integrated intensity decreases accordingly, whereas the invariant Q_δ slightly increases. This could be due to the increasing crystallization temperature, which reduces the undercooling, resulting in better-organized and thicker lamellae. In the next higher additive concentration regime a drastic decrease in both invariant and scattered intensity, as well as a dramatic change in the appearance of the scattering patterns are observed. Instead of the classical spherulite-type scattering, now a random pattern is recorded, which, at increasing concentration, gradually changes into a cross-shaped pattern with high intensities at low q values—typical for randomly arranged rod-like structures rather than spherulites.[45–48] These findings are in concert with observations made by Kobayashi and Hashimoto who reported a similar pattern in SALS studies of *i*-PP containing 0.5% w/w of agent **1**.[30] The cross-shaped pattern becomes more pronounced as the concentration of additive is increased, and the possibility that the pattern originates from the clarifying agent itself needs to be considered. However, when heating the samples to a temperature well above the melting temperature of the polypropylene, but below that of the additive, the patterns disappear at the melting temperature of the polymer. This observation indicates that the presence of the

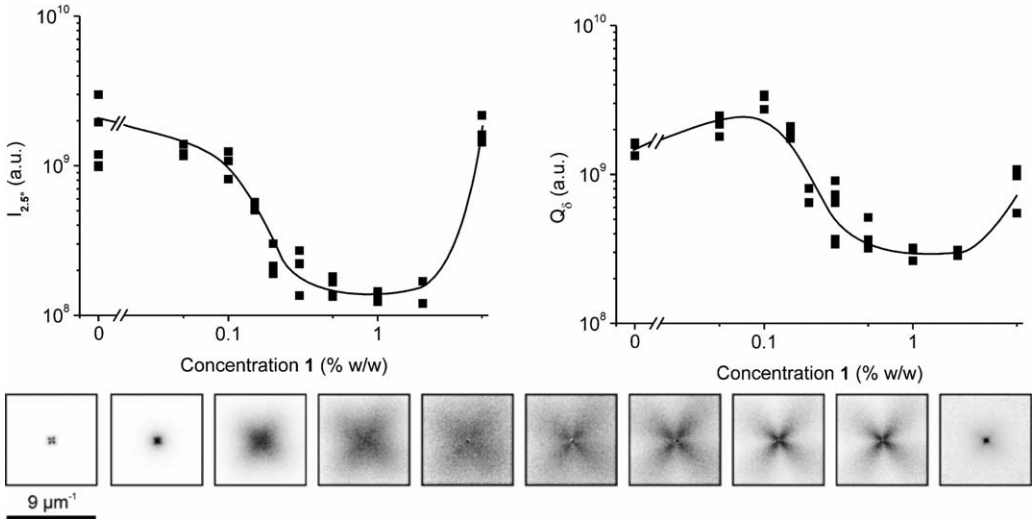

FIGURE 4 Total integrated scattering intensity at $\theta_s \geq 2.5°$ versus concentration of *i*-PP samples containing additive **1** (top left) and corresponding invariant in H_V configuration, Q_δ (top right) (The drawn lines are a guide to the eye only). Bottom: SALS images under H_V polarization for *i*-PP containing 0; 0.05; 0.1; 0.15; 0.2; 0.3; 0.5; 1.0; 2.0; and 5.0% w/w agent **1**.

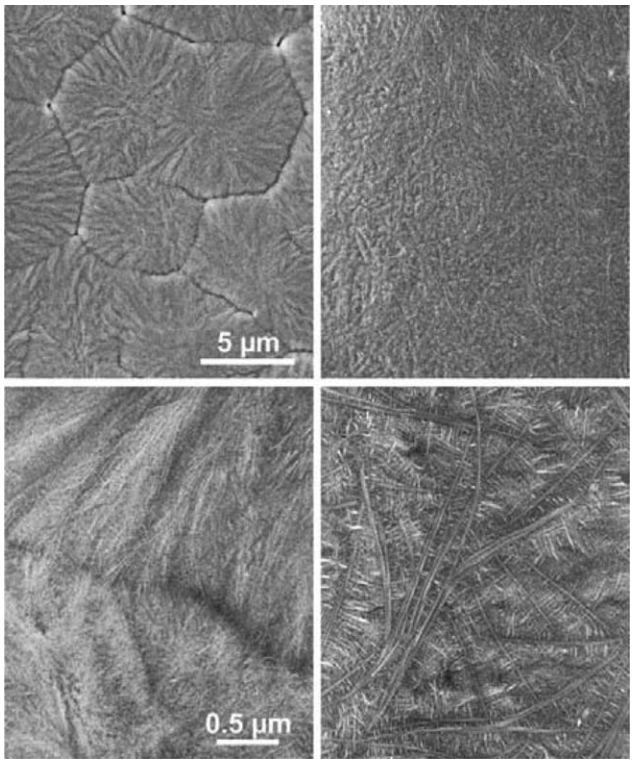

FIGURE 5 SEM images of neat *i*-PP (left) and *i*-PP containing 1% w/w of **1** (right).

solid clarifying agent in the polymer melt does not give rise to any significant scattering under crossed polarizers. By contrast, it does give rise to some scattering under parallel polarizers, indicative of fluctuations in refractive index. At concentrations $\geq 0.5\%$ w/w, the additive in the melt actually causes a larger amount of scattering than the solid mixture. Since the agent appears to give rise to more scattering in the molten polymer than in solid *i*-PP, we conclude that there is a rather good refractive index matching between **1** and the solid polymer.

Finally, at high concentrations of **1**, the region of liquid-liquid phase separation in the phase diagram is reached.[7] This is also reflected in the SALS images. The polymer blend sample containing 5% w/w of the additive features a "double pattern", i.e. an intense four-clove pattern at low q values, possibly corresponding to spherulitic scattering from *i*-PP, and a weaker pattern in the background that might relate to regions of phase-separated clarifying agent. A clear four-clove pattern from *i*-PP is only visible for the pure polymer. The maximum intensity at azimuthal angle 45° is for this pattern at $q = 0.3\ \mu m^{-1}$, corresponding to an average spherulite radius of about 13 μm (see eq 1), which compares well with optical microscopy observations.

The above observations show that **1** has its clarifying effect on *i*-PP exactly in the concentration range where the change in the appearance of the scattering pattern and the decrease in Q_δ are observed.[7] Thus, there exists an excellent correlation between the level of haze and the change in morphology of the polymer, indicating that the transformation from a spherulitic structure to a random- or rod-like arrangement is crucial and characteristic of the clarified polypropylene.

To corroborate our conclusions regarding the various morphological structures of *i*-PP, scanning electron microscopy was conducted complementary to the above SALS experiments. For this purpose, solution-cast samples of polypropylene as well as of polypropylene containing 1% w/w of **1** were produced, dried, molten and subsequently quenched. Figure 5 reveals clear, classical spherulitic structures for neat *i*-PP, whereas the polymer containing the clarifying agent features a very fine appearance comprising the fibrillar network of the additive, in accordance with earlier optical microscopy observations.[7] At increased magnification, the radially ordered lamellae constituting the spherulites in the neat *i*-PP can be discerned. The polymer lamellae in the clarified material, by contrast, are organized in rod-like shish-kebab-type structures, grown onto the fibrillar network of the clarifying agent, indeed consistent with the SALS observations presented above.

Comparison to Other Additives

In order to verify if the above transformation from classical spherulitic structures to a rod-like arrangement is more generally true for clarified *i*-PP, the morphologies of the polymer comprising two other clarifying agents, as well as of nucleated, but not clarified material were examined in the same manner. For this purpose were selected: **2**, a newer generation of the sorbitol-type clarifying agents; **3**, a commercial clarifying agent based on a core of substituted trisaminobenzene; and **4**, a substituted trisaminobenzene with nucleating, but no clarifying effect on *i*-PP (chemical structures in Table 1). In Figures 6 to 8, the evaluation of SALS data versus additive concentration, as earlier for additive **1**, is displayed for **2**, **3,** and **4**, respectively, in the relevant concentration ranges—based on the phase diagrams of the different compounds and *i*-PP.[2,5,9] Strikingly—and reassuringly—the two clarifying agents **2** and **3** both display the evolution towards random- and rod-like scattering patterns observed for **1**, with the accompanying decrease in integrated scattering intensities and invariants. As can be expected from the phase behavior and earlier haze measurements,[9] the concentration range yielding random- and rod-like patterns for *i*-PP/**2** is slightly shifted compared to that with **1**, perfectly corresponding to the compositions featuring optimal optical properties. Due to the high sensitivity to both concentration and cooling rate, the optimum composition window is smaller for the polymer containing additive **3**, and, therefore, the spread in the data is somewhat higher.

The nucleating, but nonclarifying agent **4**, on the other hand, features dominant scattering characteristics of spherulitic structures over the entire concentration range and no change into patterns characteristic of random- or rod-like arrangements was observed, as shown in Figure 8. The scattered intensity above 2.5° also does not change in the concentration range studied, in agreement with earlier studies on the

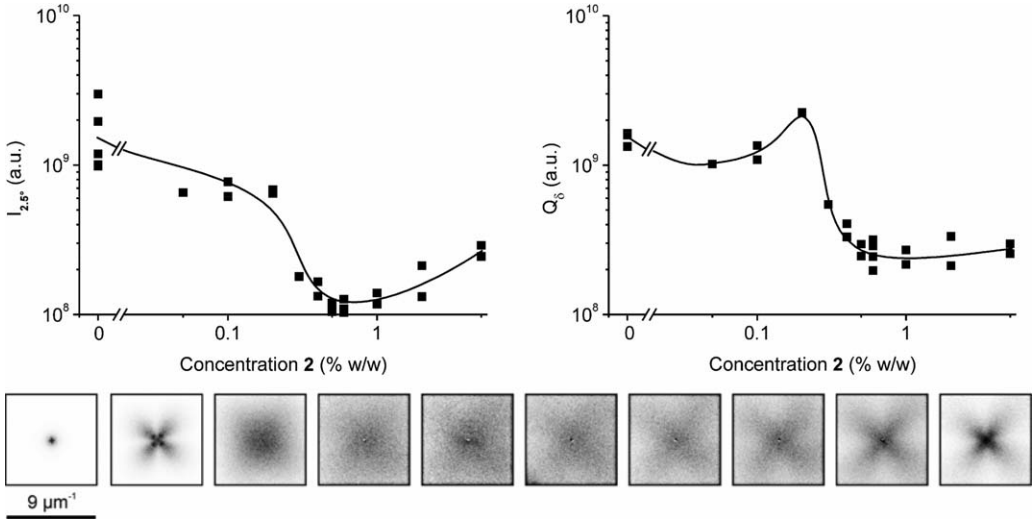

FIGURE 6 Total integrated intensity at $\theta_s \geq 2.5$ (left) and invariant in H_V (right) versus concentration of additive **2** in *i*-PP (The drawn lines are a guide to the eye only). Bottom: Corresponding SALS images under H_V polarization for *i*-PP containing: 0.05; 0.1; 0.2; 0.3; 0.4; 0.5; 0.6; 1.0; 2.0; and 5.0% w/w agent **2**.

haze of this system.[5] Interestingly, the invariant Q_δ increases slightly due to nucleation by this additive, as seen also for *i*-PP comprising small concentrations of the other agents (likely due to the decreased undercooling), but then remains constant for all other concentrations, confirming that there is no fundamental change in the solid-state structure. Results of scanning electron microscopy investigations of the above 3 *i*-PP/additive systems are presented in Figure 9. The polymer comprising the clarifying agents **2** and **3** is seen to crystallize from fibrils of the additive in the form of shish-kebab-type structures in the same manner as observed with **1**. By contrast, structures obtained with *i*-PP and the nucleating agent without clarifying ability, agent **4**, are markedly different. Although this additive forms needles similar to those of **3**, the polypropylene lamellae are not predominantly growing onto them, but rather are organized similar to those in the neat polymer, as is evident from the constant value of the invariant Q_δ. Naturally, the present spherulitic entities are significantly smaller and not as well discernable as in *i*-PP, due to nucleation of the polymer by the additive. However, the drastic change in morphology of the polymer induced by the above nucleating- and clarifying agents **1**-**3** is absent and, consequently, clarification does not take place for agent **4**. The possibly epitaxial growth of the *i*-PP chains on the fibrils evidently requires affinity of the fibril surface with the *i*-PP chains, which, combined with the large total fibril surface, explains the high nucleation density observed for these systems.[10,11]

Another interesting aspect is that the reduction in haze due to agent **2** is superior to that of the other clarifying agents, even though all agents appear to have the same shish-kebab-

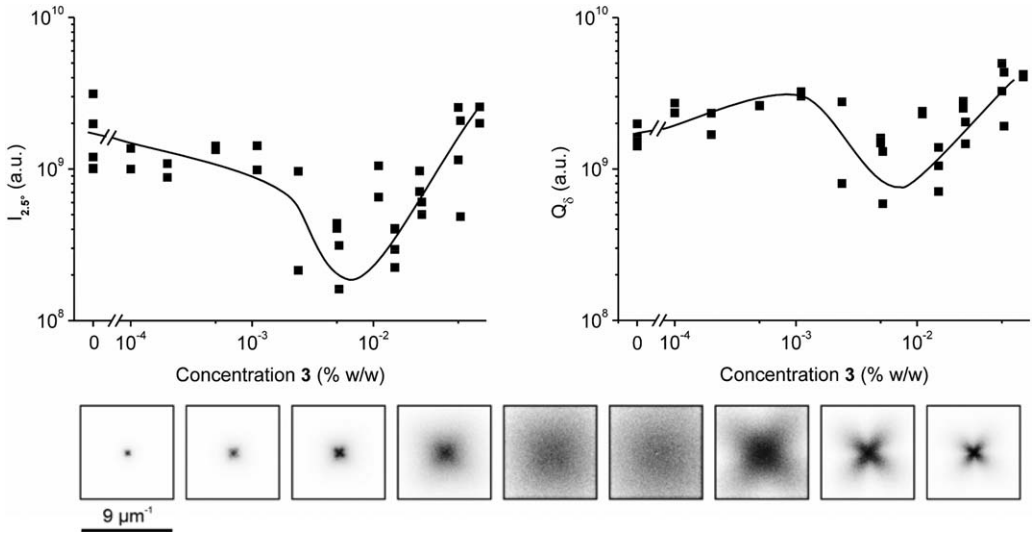

FIGURE 7 As in Figure 6 for additive **3**; corresponding SALS images under H_V polarization for *i*-PP containing: 0.0001; 0.0002; 0.0005; 0.0011; 0.0024; 0.0052; 0.011; 0.024; and 0.052% w/w agent **3**.

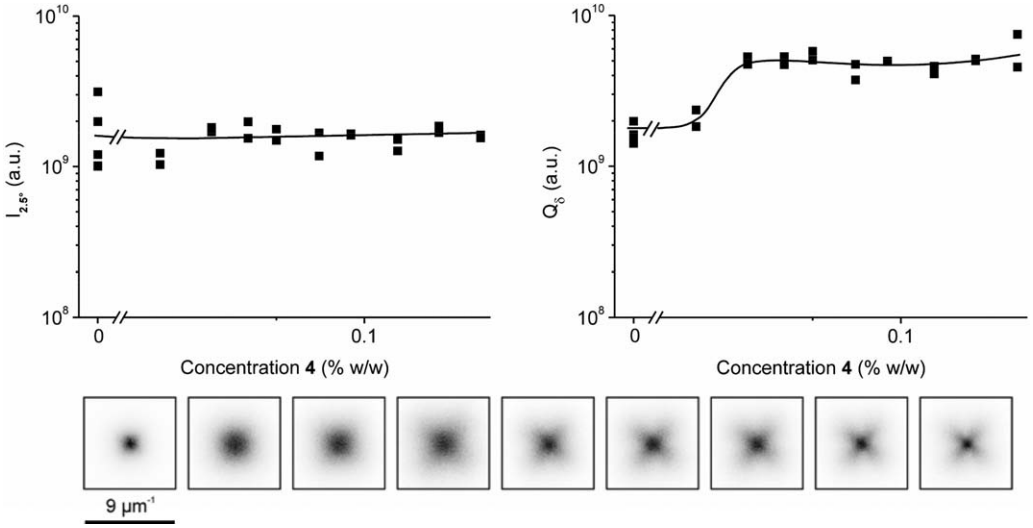

FIGURE 8 As in Figure 6 for additive **4**; corresponding SALS images under H_V polarization for *i*-PP containing: 0.02; 0.03; 0.04; 0.05; 0.07; 0.09; 0.13; 0.18; and 0.25% w/w agent **4**.

like microstructure. Upon closer examination of the SEM pictures in Figures 5 and 9, it appears that the performance of the clarifying agents **1** to **3**, as measured by their haze values in Table 1, seems to correlate with the fibril diameter of the clarifying agent, d_f, and the associated shish-kebab diameter d_s. From the SEM pictures it can be seen that

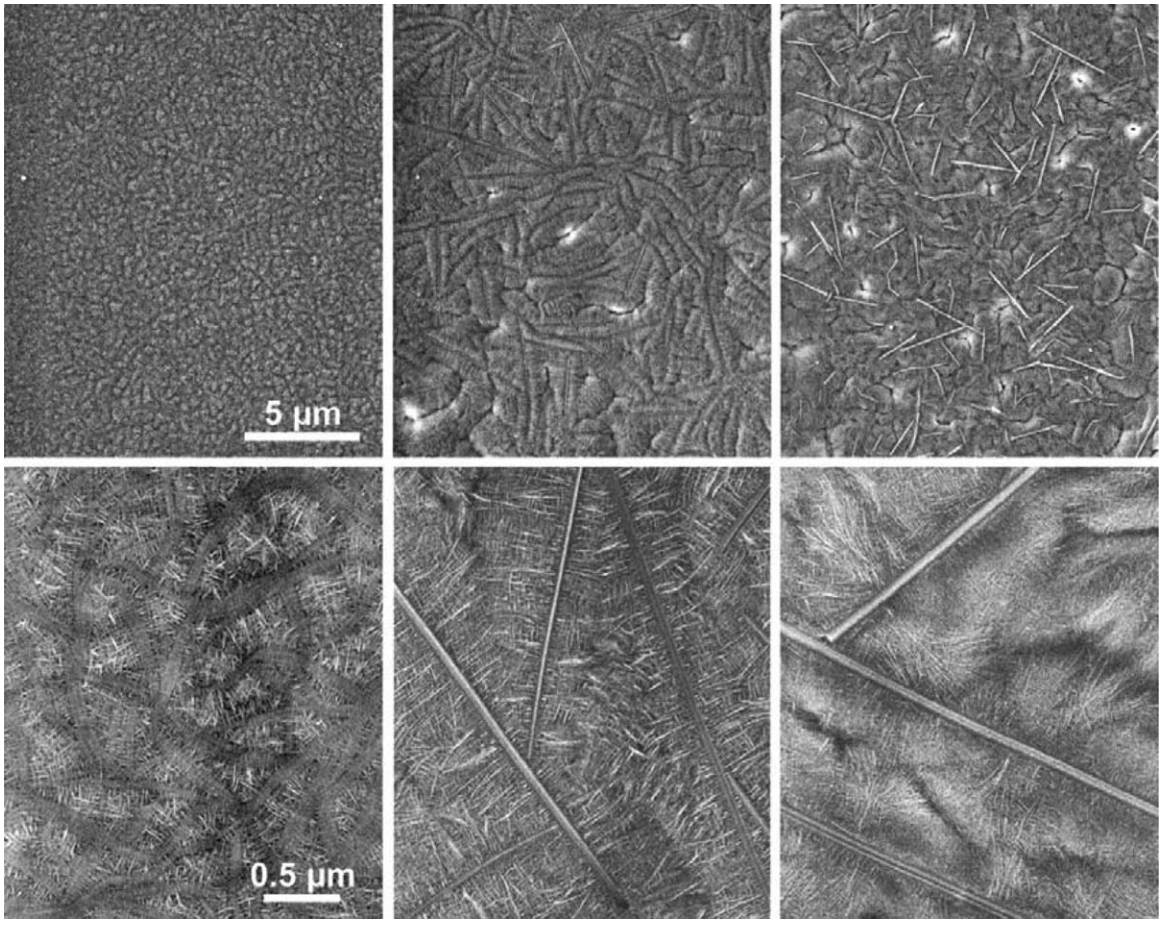

FIGURE 9 SEM images of *i*-PP at different magnification, containing 1% w/w of **2** (left), 1% w/w of **3** (center) and 2% w/w of **4** (right).

$d_f^2 < d_f^1 < d_f^3$, which corresponds to the order of the haze values listed in Table 1. This relation between haze and fibril diameter can be understood by the following argument: given a volume fraction of clarifying agent φ, which crystallizes in fibrils with diameter d_f, the total fibril length per total volume, L_f/V_{tot}, equals:

$$\varphi = \frac{V_{\text{clarifying agent}}}{V_{tot}} = \frac{\frac{\pi}{4} d_f^2 \cdot L_f}{V_{tot}} \rightarrow \frac{L_f}{V_{tot}} = \frac{4\varphi}{\pi d_f^2} \quad (5)$$

Assuming a random distribution of the fibrils, it can be shown, analogous to the dislocation density in metals, that the fibril density, defined as the number of fibrils that pierce a unit area, ρ_f, equals:[49]

$$\rho_f = \frac{1}{2} \cdot \frac{L_f}{V_{tot}} \quad (6)$$

Further assuming that the crystallization of *i*-PP onto the fibrils commences at the same time and progresses with constant speed, the shish-kebab diameter d_s will be equal to the distance between the fibrils, scaling with the fibril density as: $d_s \propto 1/\sqrt{\rho_f}$. It then follows that the diameter of the principal light-scattering units, i.e. the shish-kebabs, scale with clarifier fibril diameter and volume concentration as:

$$d_s \propto \frac{1}{\sqrt{\rho_f}} = \sqrt{\frac{\pi d_f^2}{2\varphi}} \propto \frac{d_f}{\sqrt{\varphi}} \quad (7)$$

As thinner shish-kebab structures will scatter less light, this relation suggests that the performance of (fibril-forming) clarifying agents for *i*-PP can be improved by reducing the fibril diameter and/or increasing the volume concentration of the clarifying agent. Obviously, the increase in volume fraction should then neither interfere with the phase-behavior nor with the fibril diameter. It should also be noted that scattering due to refractive index mismatching between the fibrils and the *i*-PP matrix is not considered here. Nevertheless, comparing the fibril diameters from the SEM pictures and measured optimum concentrations to the performance of the clarifying agents **1**-**3** (agent **4** does not form a shish-kebab structure and does not clarify) as measured by their haze values listed in Table 1, seems to agree favorably with the scaling relation eq 7, giving at least some guidance towards the quest of designing better clarifying agents. Finally, it should be pointed out that the undercooling, or crystallization temperature, plays a very important and complex role. On the one hand, the degree of undercooling will determine the rate of nucleation (of both the polymer and the agent). On the other hand, the crystallization temperature also directs the crystal growth rates and the lamellar thickness of the polymer. Also, the fibrillar structure of the clarifying agents is sensitive to the undercooling, with thicker nanofibril assemblies being formed at higher crystallization temperatures.[50] According to eq 7, this thickening of the nanofibrils (at constant volume fraction) will result in an increased diameter of the light-scattering shish-kebab-like structures, which, in its turn, will increase the amount of scattered light, in agreement with the observed cooling rate dependency of the clarifying ability of the agents.[7,50]

CONCLUSIONS

Combined small-angle light scattering (SALS) and scanning electron microscopy (SEM) studies on the mechanism of reducing haze in isotactic polypropylene (*i*-PP), through the addition of so-called clarifying agents reveal that a simple reduction of the size of spherulites in the solidified polymer alone cannot account for the drastic improvement of this optical characteristic. In order for an additive to achieve this, it must be capable of preventing the classical, highly efficient light scattering spherulitic structures to form in the solidifying polymer. Instead, the agent must be able to induce randomly ordered or rod- or shish-kebab-like crystalline entities. The latter requirement was suggested in literature to occur only if the additive is capable of providing a nanofibrillar scaffold with an ultra-high density of nucleation sites,[7,10,11,16] and this is directly evidenced in this study by the sudden reduction of the SALS invariant Q_δ, combined with SEM pictures of the clarified microstructure, with increasing clarifier concentration. A simple scaling law, relating the diameter of the shish-kebab structures to the fibril diameter and volume fraction of the clarifying agent is proposed, suggesting that the performance of a (fibril-forming) clarifying agent will improve by reducing the fibril diameter and/or increasing the volume concentration of the clarifying agent.

ACKNOWLEDGMENTS

We gratefully acknowledge stimulating discussions with Greg Beaucage from the University of Cincinnati and Hans-Werner Schmidt from the University of Bayreuth. We also thank Hans-Werner Schmidt for kindly supplying sample **4**.

REFERENCES AND NOTES

1 Plastics Additives Handbook; H. Zweifel, Ed.; Carl Hanser Verlag: Munich, **2001**.

2 M. Blomenhofer, S. Ganzleben, D. Hanft, H. W. Schmidt, M. Kristiansen, P. Smith, K. Stoll, D. Mader, K. Hoffmann, *Macromolecules* **2005**, *38*, 3688–3695.

3 H. Wang, C. C. Li, Y. C. Ke, D. Zhang, Z. Y. Li, *J. Appl. Polym. Sci.* **2006**, *99*, 1568–1575.

4 Y. F. Zhang, Z. Xin, *J. Appl. Polym. Sci.* **2006**, *100*, 4868–4874.

5 F. Abraham, S. Ganzleben, D. Hanft, P. Smith, H. W. Schmidt, *Macromol. Chem. Phys.* **2010**, *211*, 171–181.

6 F. Abraham, R. Kress, P. Smith, H. W. Schmidt, *Macromol. Chem. Phys.* **2013**, *214*, 17–24.

7 M. Kristiansen, M. Werner, T. Tervoort, P. Smith, M. Blomenhofer, H. W. Schmidt, *Macromolecules* **2003**, *36*, 5150–5156.

8 M. Kristiansen, A. Gress, P. Smith, D. Hanft, H. W. Schmidt, *Polymer* **2006**, *47*, 249–253.

9 K. Bernland, T. Tervoort, P. Smith, *Polymer* **2009**, *50*, 2460–2464.

10 A. Menyhárd, M. Gahleitner, J. Varga, K. Bernreitner, P. Jaaskelainen, H. Oysaed, B. Pukánszky, *Eur. Polym. J.* **2009**, *45*, 3138–3148.

11 Z. Horváth, B. Gyarmati, A. Menyhárd, P. Doshev, M. Gahleitner, J. Varga, B. Pukánszky, *RSC Adv.* **2014**, *4*, 19737–19745.

12 A. S. Vaughan, I. L. Hosier, *J. Mater. Sci.* **2007**, *43*, 2922–2928.

13 A. Nogales, G. R. Mitchell, *Polymer* **2005**, *46*, 5615–5620.

14 A. Nogales, R. H. Olley, G. R. Mitchell, *Macromol. Rapid Commun.* **2003**, *24*, 496–502.

15 A. Nogales, S. A. Thornley, G. R. Mitchell, *J. Macromol. Sci. Part B: Phys.* **2004**, *43*, 1161–1170.

16 J. Lipp, M. Shuster, A. E. Terry, Y. Cohen, *Langmuir* **2006**, *22*, 6398–6402.

17 M. Schmidt, J. J. Wittmann, R. Kress, H. W. Schmidt, J. Senker, *Chem. Commun. (Camb.).* **2013**, *49*, 267–269.

18 E. Andreassen, A. Larsen, K. Nord-Varhaug, M. Skar, H. Oysaed, *Polym. Eng. Sci.* **2002**, *42*, 1082–1097.

19 A. Misra, R. S. Stein, *J. Polym. Sci. Part B: Polym. Lett.* **1972**, *10*, 473–477.

20 Z. Bartczak, A. Galeski, *Polymer* **1990**, *31*, 2027–2038.

21 T. Okada, H. Saito, T. Inoue, *Macromolecules* **1992**, *25*, 1908–1911.

22 C. H. Lee, H. Saito, T. Inoue, *Macromolecules* **1993**, *26*, 6566–6569.

23 N. V. Pogodina, S. K. Siddiquee, J. W. van Egmond, H. H. Winter, *Macromolecules* **1999**, *32*, 1167–1174.

24 Z. G. Wang, B. S. Hsiao, E. B. Sirota, P. Agarwal, S. Srinivas, *Macromolecules* **2000**, *33*, 978–989.

25 Z. C. Xiao, Y. A. Akpalu, *Polymer* **2007**, *48*, 5388–5397.

26 J. Baert, P. Van Puyvelde, *Macromol. Mater. Eng.* **2008**, *293*, 255–273.

27 U. Johnsen, G. Spilgies, *Angew. Makromol. Chem.* **1973**, *31*, 123–135.

28 S. N. Garg, R. S. Stein, T. K. Su, R. J. Tabar, A. Misra, In International Topical Conference on Kinetics of Aggregation and Gelation; F. Family; D. P. Landau, Eds.; North-Holland: Athens, GA, **1984**; pp 229–234.

29 S. Garg; R. Stein, In ANTEC; Atlanta, GA, **1988**; pp 1021–1025.

30 T. Kobayashi; T. Hashimoto, *Bull. Chem. Soc. Jpn.* **2005**, *78*, 218–235.

31 C. Xie; J. Li; J. Xia, WO PCT/US2005/035635, **2006**.

32 H. S. Bu, S. Z. D. Cheng, B. Wunderlich, *Makromol. Chem. Rapid Commun.* **1988**, *9*, 75–77.

33 F. M. Willmouth, In Optical Properties of Polymers; G. H. Meeten, Ed.; Elseviers Applied Science Publishers: London, **1986**.

34 M. Prusty, B. J. Keestra, J. G. P. Goossens, P. D. Anderson, *Chem. Eng. Sci.* **2007**, *62*, 1825–1837.

35 R. l'Abee, H. Goossens, M. van Duin, *Polymer* **2008**, *49*, 2288–2297.

36 R. S. Stein, J. J. Keane, *J. Polym. Sci.* **1955**, *17*, 21–44.

37 G. B. Airy, *Trans. Cambridge Philos. Soc.* **1838**, *6*, 379–403.

38 G. Mie, *Ann. Phys.* **1908**, *25*, 377–445.

39 R. S. Stein, M. B. Rhodes, *J. Appl. Phys.* **1960**, *31*, 1873–1884.

40 D. Y. Yoon, R. S. Stein, *J. Polym. Sci. Part B: Polym. Phys.* **1974**, *12*, 735–761.

41 A. P. Hammersley, S. O. Svensson, M. Hanfland, A. N. Fitch, D. Hausermann, *High Pressure Res.* **1996**, *14*, 235–248.

42 J. Koberstein, T. P. Russell, R. S. Stein, *J. Polym. Sci. Part B: Polym. Phys.* **1979**, *17*, 1719–1730.

43 Y. A. Akpalu, Y. Y. Lin, *J. Polym. Sci. Part B: Polym. Phys.* **2002**, *40*, 2714–2727.

44 M. Peeters, B. Goderis, C. Vonk, H. Reynaers, V. Mathot, *J. Polym. Sci. Part B: Polym. Phys.* **1997**, *35*, 2689–2713.

45 M. Moritani, N. Hayashi, A. Utsuo, H. Kawai, *Polym. J.* **1971**, *2*, 74–87.

46 R. E. Prudhomme, R. S. Stein, *J. Polym. Sci. Part B: Polym. Phys.* **1974**, *12*, 1805–1823.

47 T. Hashimoto, Y. Murakami, H. Kawai, *J. Polym. Sci. Part B: Polym. Phys.* **1975**, *13*, 1613–1631.

48 J. Maxfield, L. Mandelkern, *Macromolecules* **1977**, *10*, 1141–1153.

49 G. Schoeck, *J. Appl. Phys.* **1962**, *33*, 1745.

50 T. Meijer-Vissers, H. Goossens, *Macromol. Symp.* **2013**, *330*, 150–165.

51 Y. Akpalu, L. Kielhorn, B. S. Hsiao, R. S. Stein, T. P. Russell, J. van Egmond, M. Muthukumar, *Macromolecules* **1999**, *32*, 765–770.